Journal of the Indian Society of Remote Sensing (May 2020) 48(5):709–720
https://doi.org/10.1007/s12524-019-01068-5

RESEARCH ARTICLE

Analysis of Surface Reflectance Retrieval Over Four Typical Surfaces Via Gaofen-1 Satellite WFV4 Imagery

Hong Guo[1] · Xingfa Gu[1] · Fangwen Bao[1] · Shuaiyi Shi[1]

Received: 26 March 2019 / Accepted: 31 October 2019 / Published online: 13 March 2020

Abstract
As a basis for the quantitative application of satellite remote sensing, surface reflectance can be retrieved through atmospheric correction methods. Currently, most studies have focused on developing or comparing atmospheric correction methods. However, few studies have quantitatively analyzed the effects of input parameters in an atmospheric correction method on retrieved surface reflectance. In this study, we evaluated the effects of the calibration coefficient, aerosol optical depth (AOD), aerosol type, and satellite zenith angle over four typical surfaces using wide field-of-view sensor four data of the Gao Fen-1 satellite. The results showed that (1) the relative errors of shrub, corn, grass, and soil reflectance increased as the calibration coefficient error increased; (2) the calibration coefficient, AOD, aerosol type, and satellite zenith angle affected corn reflectance retrieval the most, whereas they had the smallest effect on soil reflectance retrieval; and (3) the accuracy of the satellite zenith angle on the retrieved surface reflectance was the least pronounced, whereas the accuracy of aerosol type was the most pronounced.

Keywords Remote sensing · Surface reflectance · Aerosols · Calibration · Spectra

Introduction

Passive satellite remote sensing is widely used to monitor the Earth's surface, resources, and atmosphere due to its broad spatial coverage and high temporal resolution (Qin et al. 2015; Zhang et al. 2019a, b). However, accurate land surface reflectance data, which the atmosphere often contaminates, are needed to fully realize the potential of these applications (Shao et al. 2018; Zou et al. 2019). Thus, surface reflectance should be obtained using atmospheric correction (Cheng et al. 2009; Zou et al. 2015).

To acquire accurate surface reflectance data, three primary types of atmospheric correction methods have already been developed. The first type includes image-based atmospheric correction methods, such as the dark-object subtraction method (Chavez 1996; Tian et al. 1998). The second type, the historical empirical line method, is necessary for measuring the reflectance spectra of calibration targets on the ground with a field spectrometer (Baugh and Groeneveld 2008; Vaudour et al. 2008). The third type includes radiative transfer models, such as the 6SV, MODTRAN, and RT3 models (Vermote et al. 1997; Berk 1999; Evans and Stephens 1991; Wang et al. 2016). In addition, studies have evaluated the performance of different atmospheric correction methods (Mahiny and Turner 2007; Clark et al. 2010; Chrysoulakis et al. 2010; Tyagi and Bhosle 2011; Guo et al. 2014). Although studies have shown that the dark-object subtraction or historical empirical line methods perform better in a specific area and at a particular time, the radiative transfer models have been widely used to retrieve surface reflectance (Vermote and Vermeulen 1999; Vermote and Kotchenova 2008; Li et al. 2011).

Many input parameters in atmospheric correction methods affect the accuracy of surface reflectance data retrieved from satellite observations. For example, the calibration coefficient translates the DN value to reflectance at the top of atmosphere (TOA). Due to atmosphere–surface radiative interactions, AOD directly reflects the

✉ Hong Guo
guohong@radi.ac.cn

Xingfa Gu
guxingfa@radi.ac.cn

[1] State Key Laboratory of Remote Sensing Science, Institute of Remote Sensing and Digital Earth, Chinese Academy of Sciences, Beijing, China

quality of the atmospheric environment. Aerosol type determines the function of atmospheric path radiance and atmospheric transmittance, and the satellite zenith angle affects the amount of scattering and absorption of gas in the atmosphere on the reflective path. However, few studies have quantitatively analyzed the effects of these parameters on retrieved surface reflectance. Therefore, the purpose of this study was to evaluate the effects of these parameters on retrieved surface reflectance via Gao Fen-1 (GF-1) satellite wide field-of-view sensor four (WFV4) imagery.

Data and Methods

GF-1 Satellite WFV4 Camera and Observation Experiments

GF-1 is the first satellite of the Chinese high-resolution Earth observing system, which was successfully launched from the Jiuquan Satellite Launch Center in April 2013. The payloads of the GF-1 satellite contain four wide field-of-view imagers (WFV1, WFV2, WFV3, and WFV4). We obtained the calibration coefficient (gain) and solar exoatmospheric irradiance (E_0) of the GF-1 satellite WFV4 camera. (Table 1) (Bai 2014; Gu and Tong 2015; Gao et al. 2016).

We conducted a comprehensive experiment in Zhangjiakou city from September 11 to 20, 2015. We observed the AOD with a CIMEL Electronique 318 spectral radiometer. Shrub, grass, corn, and soil represent typical surfaces and are widely used in the quantitative application of remote sensing. Therefore, we observed the spectra of these four surfaces from uniform flat surfaces using an Analytica Spectra Devices (ASD) field spectrometer with a spectral range from 350 to 2500 nm. We selected the four surfaces of a GF-1 satellite WFV4 camera on September 14, 2015, to analyze the effects of input parameters in atmospheric correction methods on retrieved surface reflectance.

Methods

The 6SV Model

The upward reflectance at the TOA and the surface reflectance of the Lambertian ground surface under a plane-parallel atmosphere can be described using the function in Eq. (1) (Vermote and Kotchenova 2008):

$$\rho_{\lambda}^{s}(\theta_s,\theta_v,\varphi)=\frac{\rho_{\mathrm{TOA}}(\theta_s,\theta_v,\varphi)-\rho_0(\theta_s,\theta_v,\varphi)}{F_{\lambda}(\theta_s)T_{\lambda}(\theta_v)+\rho_{\mathrm{TOA}}(\theta_s,\theta_v,\varphi)S-\rho_0(\theta_s,\theta_v,\varphi)S} \quad (1)$$

where $\theta_s, \theta_v,$ and φ represent the solar zenith, satellite zenith, and relative azimuth angles, respectively, F_{λ} is the normalized downward flux for zero surface reflectance, T_{λ} represents the upward total transmission, S is the atmospheric backscattering ratio, ρ_0 is the atmosphere intrinsic reflectance, ρ_{λ}^{s} is the Lambertian angular spectral surface reflectance at wavelength λ, and ρ_{TOA} stands for the reflectance at the TOA and is calculated using Eqs. (2) and (3):

$$L = DN \times \mathrm{Gain} + \mathrm{Bias} \quad (2)$$

$$\rho_{\mathrm{TOA}} = \frac{L\pi d^2}{E_0 \cos\theta_s} \quad (3)$$

where L is the TOA radiance of a GF-1 WFV4 image, DN is the value of GF-1 WFV4 observations, Gain is the radiance calibration coefficient, d is the ratio of average Sun–Earth distance and transit distance of the satellite between Sun and Earth (Wang et al. 2016), and E_0 is the solar exoatmospheric irradiance.

The 6SV model is an advanced radiative transfer model that is specifically designed to simulate a coupled atmosphere–surface system's reflection of radiation. The accuracy of the 6SV model is stated to be within 1%, which complies with the accuracy requirements of standard radiative transfer codes, and the accuracy of the MOD09 surface reflectance product has been significantly improved due to the use of the 6SV model (Vermote and Vermeulen 1999; Vermote and Kotchenova 2008). Therefore, we used the 6SV model to evaluate the effects of input parameters in atmospheric correction methods on retrieved surface reflectance. By inputting the important parameters (e.g., aerosol type, AOD, sun zenith and azimuth angles, satellite zenith and azimuth angles, date and time of image acquisition) in the 6SV model, we produced accurate surface reflectance following atmospheric correction. In the present study, we applied the 6SV model to GF-1 WFV4 imagery and performed a sensitivity analysis of the effects of input parameters in atmospheric correction methods on retrieved surface reflectance. The original input parameters in the 6SV model are shown in Table 2.

Table 1 Gain and exoatmospheric solar constant of GF-1 satellite WFV4 camera

GF-1 WFV4	Band 1	Band 2	Band 3	Band 4
Gain (DN/W m^{-2} sr^{-1} μm^{-1})	0.2014	0.179	0.163	0.1533
Bias (W m^{-2} sr^{-1} μm^{-1})	0	0	0	0
E_0 (W m^{-2} μm^{-1})	1966.08	1838.80	1538.36	1069.55

Table 2 The input values for parameters in the 6SV model

Solar zenith angle	Solar azimuth angle	Satellite zenith angle	Satellite azimuth angle	Aerosol type	AOD
36.675	174.079	26.613	285.386	Continental	0.4

Spectrum Convolution Function

ASD-measured surface reflectance can be converted to the reflectance of a WFV4 image using the function in Eq. (4):

$$\rho_i = \frac{\int \rho(\lambda)\psi_i(\lambda)\mathrm{d}\lambda}{\int \psi_i(\lambda)\mathrm{d}\lambda} \quad (4)$$

where ρ_i is the reflectance at band i of a WFV4 image, $\rho(\lambda)$ is the reflectance measured with the ASD field spectrometer, and $\psi_i(\lambda)$ is the spectrum at band i of the WFV4 camera.

Relative Error

Relative error (RE) is widely used to evaluate the accuracy of models, etc. In the present study, we calculated the RE to evaluate the effects of the calibration coefficient, AOD, aerosol type, and the satellite zenith angle in atmospheric correction methods on retrieved surface reflectance. RE was defined using the function in Eq. (5):

$$\mathrm{RE} = \frac{x - y}{y} \times 100\% \quad (5)$$

where, when evaluating the effects of input parameters in atmospheric correction methods on retrieved surface reflectance, x represents the predicted surface reflectance, produced by running the 6SV model with one input parameter changed each time; meanwhile, y represents the fixed surface reflectance, calculated by running the 6SV model with the input parameters shown in Table 2. However, when evaluating the difference in reflectance between the WFV4 camera and Moderate resolution Imaging Spectroradiometer (MODIS), x represents the surface reflectance of MODIS, and y represents the surface reflectance of the WFV4 camera, calculated based on the convolution of the WFV4 camera spectra, MODIS spectra, and ASD-measured surface reflectance, respectively.

Results

The Effects of Calibration Coefficient Accuracy on Surface Reflectance Retrieval

The China Center for Resources Satellite Data and Application (CCRSDA) provided the calibration coefficients of the GF-1 satellite, where the errors are mainly at ± (3–7%) (Yang et al. 2015; Li et al. 2016). Therefore, to evaluate the effects of calibration coefficient accuracy on retrieved surface reflectance, we increased the calibration coefficient by 3% and 7% and decreased the calibration coefficient by 3% and 7%, respectively (Fig. 1).

The results indicated that the REs of four types of surface reflectance increased as the calibration coefficient error increased (Fig. 1). Compared with the four surfaces (e.g., band 1), when the calibration coefficient increased by 3% and 7%, the REs of corn reflectance exhibited the greatest increases of 33.3% and 80.0%, respectively, whereas the REs of soil reflectance increased the least at 8.3% and 20.2%, respectively. In addition, the RE of band 1 shrub reflectance had the greatest increase (20.0%), whereas the RE of band 4 shrub reflectance increased the least (2.8%).

Compared with the 3% increase in the calibration coefficient, when the calibration coefficient increased by 7% (e.g., shrub), the REs of bands 1, 2, 3, and 4 of surface reflectance increased by a factor of ~ 2.5 (52%/20% = 2.6, 18%/8.2% = 2.2, 11.4%/4.3% = 2.7, 7.3%/2.8% = 2.6, respectively). The variation was almost same for the other three surfaces.

This was because when the calibration coefficient increased, the reflectance at the TOA also increased. Therefore, if the effects of atmosphere is a constant value, a higher reflectance at the TOA will result in a higher real surface reflectance. Thus, compared with the standard values, the REs increased as the calibration coefficient increased. Furthermore, the different extinction effects of the atmosphere and the different surface reflectance for each band accounted for the REs of band differences.

The Effects of AOD Accuracy on Surface Reflectance Retrieval

The AOD products known as MOD04 C5/C6 are widely used for atmospheric correction, and their expected error is ± (0.05 + 0.15 × AOD) over land when quality assurance is high (confidence = 3) (Levy et al. 2010, 2013). Therefore, to analyze the effects of AOD accuracy on retrieved surface reflectance, we changed the AOD (0.4) with the expected error (Fig. 2).

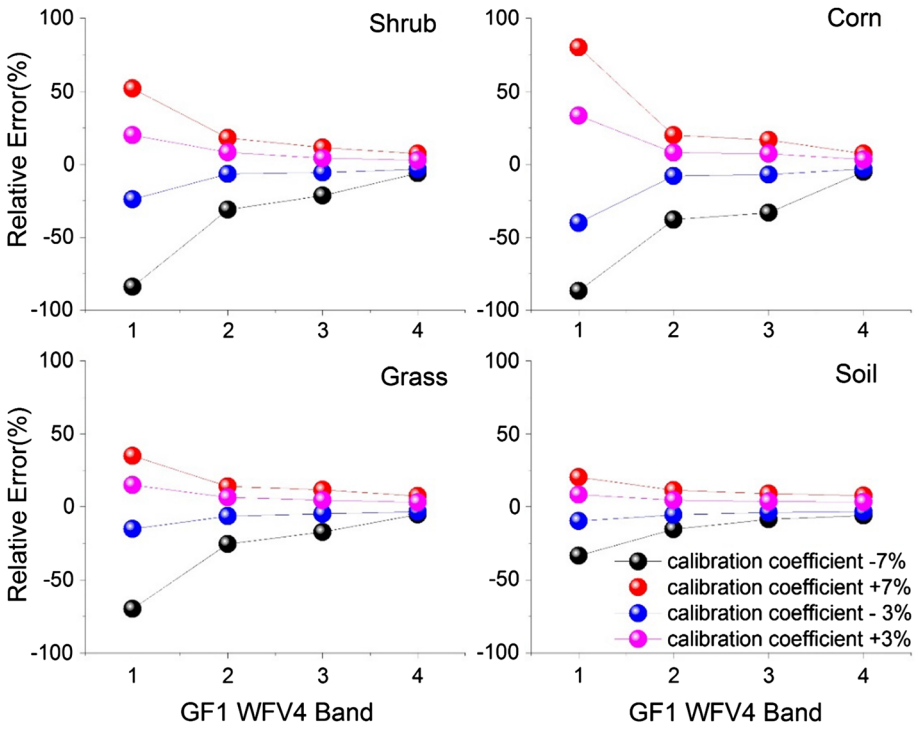

Fig. 1 The effects of calibration coefficient accuracy on the retrieved surface reflectance

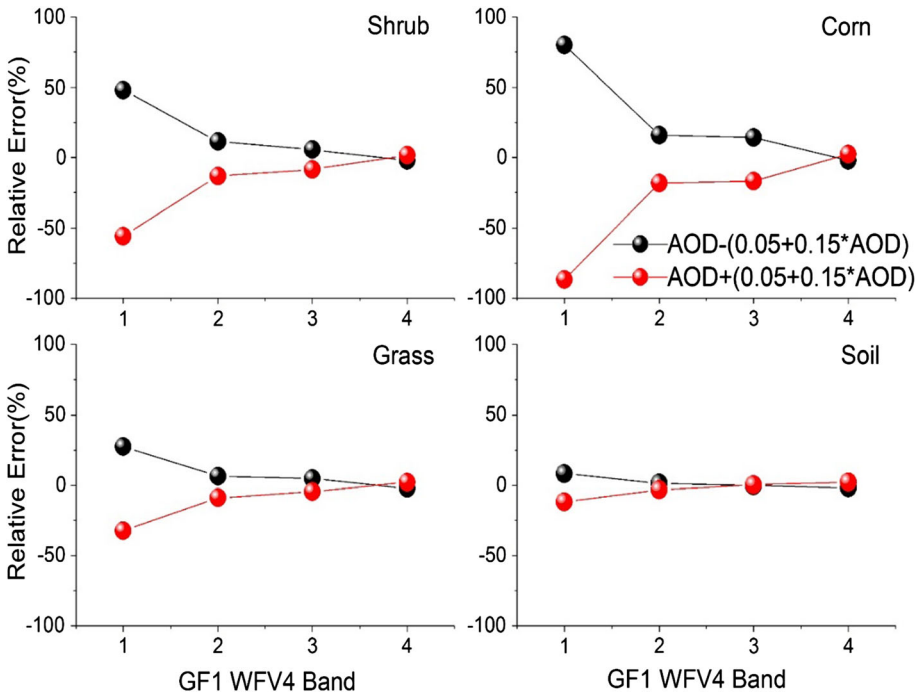

Fig. 2 The effects of AOD accuracy on the retrieved surface reflectance

Compared with the four surfaces (e.g., band 1), when the AOD increased by 0.05 + 0.15 × AOD, the RE of corn reflectance exhibited the greatest decrease (− 86.7%), followed by the RE of shrub reflectance (− 56.0%). Meanwhile, grass had a relatively low decrease in reflectance (− 32.5%), and the RE of soil reflectance decreased the least (− 11.9%; Fig. 2). In addition, the RE of band 1 shrub reflectance decreased the most (− 56.0%), whereas the RE of band 4 shrub reflectance decreased the least (1.6%).

Compared with the increase in the error of AOD, when the AOD decreased by 0.05 + 0.15 × AOD (e.g., shrub), the REs of the surface reflectance of bands 1, 2, 3, and 4 showed the opposite variations (48%, 11.48%, 5.71%,

− 2.0%, respectively), which was almost same for the other three surfaces. This occurred because the extinction effects of aerosols were strong in the visible spectrum and weak in the near-infrared spectrum, and the because of the different surface reflectance for each band.

The Effects of Aerosol Type Accuracy on Surface Reflectance Retrieval

The aerosol types that the 6SV model provides, including urban, biomass burning, dust, continental, and oceanic aerosols, are widely used in the retrieval of surface reflectance. Lee and Kim (2010) also proposed six aerosol types (cluster 1, cluster 2, cluster 3, cluster 4, cluster 5, and cluster 6) based on the analysis of Asian aerosols, and cluster 6 is referred to as dusty aerosols. In addition, Zhangjiakou has a mid-latitude continental climate. Therefore, we used urban, biomass burning, continental, and cluster 6 aerosol types to evaluate the effects of aerosol type accuracy on retrieved surface reflectance (Fig. 3).

When the aerosol type was urban, the REs of band 4 surface reflectance for shrub, corn, grass, and soil exhibited the smallest variations (13.0%, 13.3%, 13.1%, and 13.2%, respectively), followed by bands 3 and 2 with larger changes. However, for band 1, the four types of surface reflectance fluctuated dramatically, with the REs of 184%, 286.7%, 122.5%, and 71.4%, respectively (Fig. 3).

When the aerosol type was biomass burning, the REs of the four types of surface reflectance were small. For corn, shrub, and grass, the REs of band 1 surface reflectance exhibited the largest variations, with values of 40.0%, 20.0%, and 12.5%, respectively. Thus, band 3 surface reflectance decreased the least, with values of − 2.4%, − 4.3%, and − 3.4%, respectively. For soil, the RE of band 2 surface reflectance decreased the most (− 7.6%); thus, the RE of band 1 surface reflectance exhibited the smallest variation (2.4%).

When the aerosol type was cluster 6, the REs of band 1 surface reflectance for shrub, corn, grass, and soil were bigger than those of biomass burning aerosol type and thus smaller than those of urban aerosol type. Besides, the REs of the other three bands' surface reflectance exhibited the similar variations to those of urban aerosol type.

This may be because the different percentages of components (e.g., dust, water-soluble, marine, and soot particles) among urban, biomass burning, continental, and cluster 6 aerosol types, which led to different levels of atmosphere reflectance (Vermote and Kotchenova 2008). Shorter wavelength resulted in larger aerosol reflectance, leading to the different REs on the retrieved surface reflectance.

The Effects of Satellite Zenith Angle Accuracy on Surface Reflectance Retrieval

The view angle of the WFV4 camera was approximately 16°. However, we could obtain only a satellite zenith angle and other geometric data under the center for one image. The maximum difference in satellite zenith angle between the center and the edge of one image was about 8° (Wang et al. 2015), therefore, we evaluated the effects of satellite zenith angle accuracy on retrieved surface reflectance (increased by 8° and decreased by 8°, respectively).

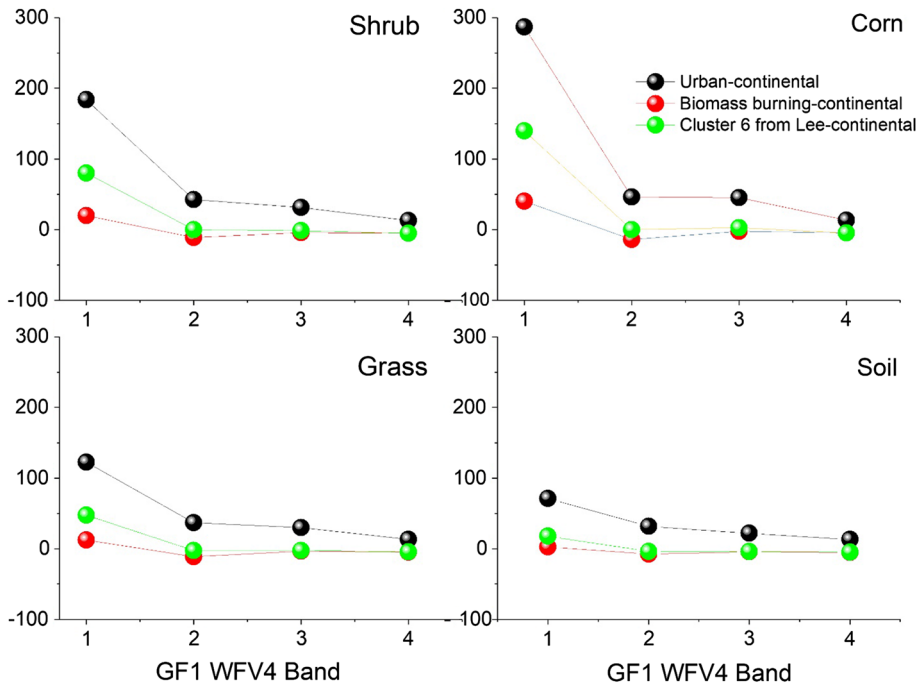

Fig. 3 The effects of aerosol type accuracy on the retrieved surface reflectance

When the satellite zenith angle increased by 8°, the REs of band 1 surface reflectance for shrub, corn, grass, and soil corresponded with the largest variation (− 32.0%, − 53.3%, − 17.5%, and − 8.3%, respectively; Fig. 4). Thus, the REs of band 4 surface reflectance exhibited almost no variation (0.0%, 0.3%, 0.3%, and 0.0%).

In addition, when the satellite zenith angle decreased by 8°, the REs of surface reflectance for the four surfaces exhibited the similar variations to those of the satellite zenith angle that increased by 8°. The REs of band 1 surface reflectance for shrub, corn, grass, and soil featured the greatest variation (12.0%, 26.7%, 7.5%, and 2.4%, respectively). However, the REs of band 4 surface reflectance exhibited almost no variation (− 0.4%, − 0.3%, − 0.3%, and 0.0%).

This was because when the satellite zenith angle decreased, it reduced the distance at which the target pixel radiation was transmitted in the atmosphere, thereby reducing the extinction effects of the atmosphere nevertheless, the extinction effects of atmosphere were different for each band.

Discussion

Validation of the Atmospheric Correction Method

In this paper, the atmospheric correction method was developed based on the 6SV model. In order to quantitatively evaluate the accuracy of atmospheric correction method, we compared the results of atmospheric correction method with ASD-measured surface reflectance. Because of the high spatial resolution of GF-1/WFV4 surface reflectance, surface reflectance of pure pixels, named shrub, corn, grass, and soil, can be directly validated (Fig. 5). The results indicated that the surface reflectance for shrub, corn, grass, and soil exhibited small variations with ASD-measured surface reflectance. The absolute errors (AEs) of band 1 for the four surfaces were the smallest, while those of band 4 were the largest. Compared with the four surfaces, the accuracy of shrub surface reflectance was the highest, followed by corn and grass surface reflectance, while those of soil surface reflectance were the lowest.

In addition, we also compare the results of atmospheric correction method with MOD09 surface reflectance. The spatial resolution of 500 m MOD09 on September 14, 2015, was used to analyze. Then, we use MODIS Reprojection Tool Swath to set it with the Geographic Lat/Lon projection, which is the same with the projection of GF-1/WFV4 surface reflectance. Further, the spatial resolution of GF-1/WFV4 surface reflectance was resampled to 500 m, and the same areas from MOD09 were extracted via GF-1/WFV4 surface reflectance image.

Because the spatial resolution of MOD09 is 500 m, which may contain many mixed pixels, and the mixed pixels would result in the uncertainties for validation surface reflectance (Li et al. 2011; Wang et al. 2016); therefore, in order to minimize the influence of mixed pixels on the evaluation of atmospheric correction method, we

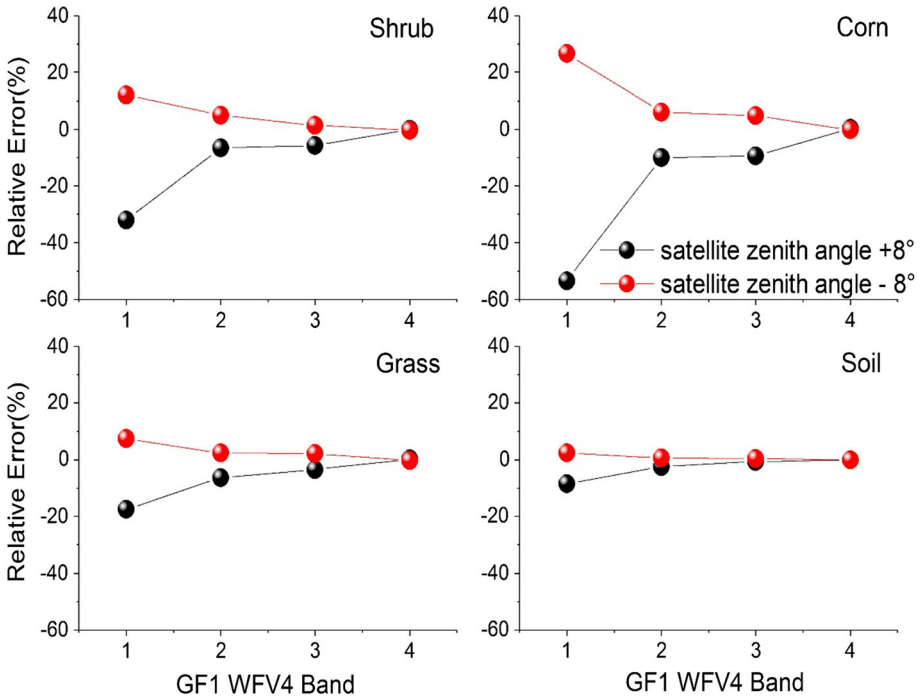

Fig. 4 The effects of satellite zenith angle accuracy on the retrieved surface reflectance

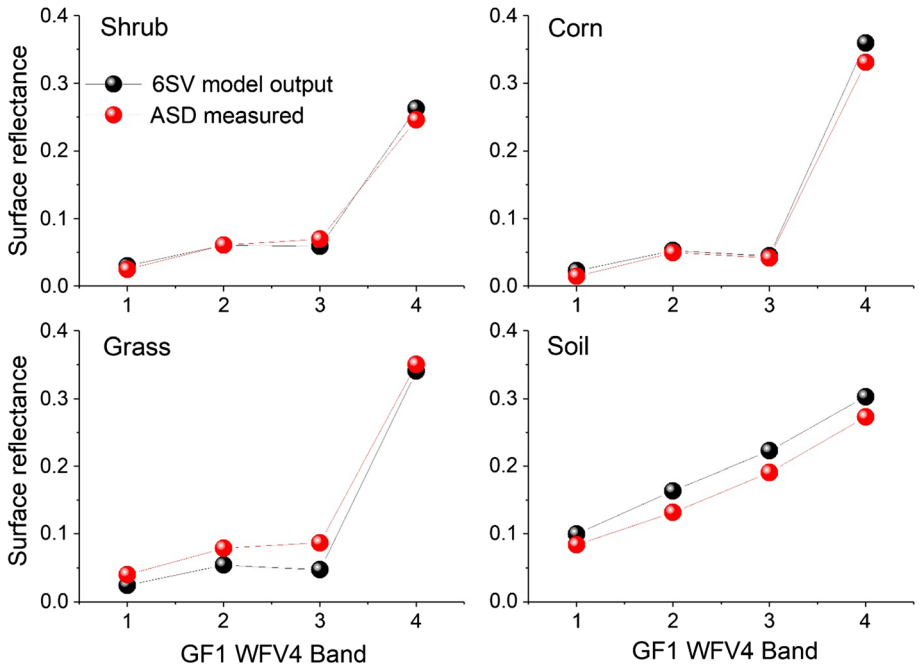

Fig. 5 Validation of the atmospheric correction method via ASD-measured surface reflectance

selected three relative homogeneous areas (brae, farmland, and city) from MOD09 and GF-1/WFV4, which were colored with the red rectangles in Fig. 6a. As Fig. 6 shows, the correlations for four bands surface reflectance from brae and farmland exhibited good consistency between MOD09 and GF-1/WFV4. However, there were differences for band 3 and band 4 from city between them. From Fig. 6a, we can find the homogeneity of bare and farmland is better than that of city, which may be the reason for the difference of validation results (Li et al. 2011; Wang et al. 2016). Overall, the developed atmospheric correction method was effective for GF-1/WFV4 image.

Analysis of the variations of REs for the surface reflectance

This paper evaluated the effects of the calibration coefficient, AOD, aerosol type, and satellite zenith angle on retrieved surface reflectance over four typical surfaces via GF-1 satellite WFV4 imagery. The results showed that the REs of four types of surface reflectance increased as the calibration coefficient error increased. The calibration coefficient, AOD, aerosol type, and satellite zenith angle had the largest effects on corn reflectance retrieval, whereas they had the smallest effects on soil reflectance retrieval. By taking the effects of AOD accuracy on retrieved surface reflectance as an example (Table 3), we found that the absolute errors for all of the surfaces were small. In addition, the REs were more sensitive for low levels of surface reflectance than for high levels of surface reflectance. This supports the statement that "the AOD affects corn reflectance retrieval the largest, whereas it had the smallest impact on soil reflectance retrieval."

Furthermore, the effects of sun zenith angle accuracy and azimuth angle accuracy on surface reflectance retrieval were also analyzed. Because the maximum difference in sun zenith angle from GF-1/WFV4 image was about 1° (Wang et al. 2015), we evaluated the effects of sun zenith angle accuracy on retrieved surface reflectance (increased by 1° and decreased by 1°, respectively). The results indicated that the REs of four types of surface reflectance were all very small ("Appendix C"), with the maximum REs of 6.7% and − 6.7% for corn when the sun zenith angle increased by 1° and decreased by 1°, respectively, and therefore, the errors from sun zenith angle for GF-1/WFV4 atmospheric correction can be ignored. In addition, because the maximum difference in azimuth angle from GF-1/WFV4 image was about 10° (Wang et al. 2015), we evaluated the effects of azimuth angle accuracy on retrieved surface reflectance (increased by 10° and decreased by 10°, respectively). When the azimuth angle increased by 10°, the REs of band 1 surface reflectance for shrub, corn, grass, and soil corresponded with the largest variation (12.0%, 20.0%, 7.5%, and 2.4%, respectively). Thus, the REs of band 4 surface reflectance exhibited no variation ("Appendix D"). Besides, when the azimuth angle decreased by 10°, the REs of surface reflectance for the four surfaces exhibited the similar variations to those of the azimuth angle that increased by 10°. Therefore, the errors from azimuth angle for GF-1/WFV4 atmospheric correction should be considered, especially for band 1.

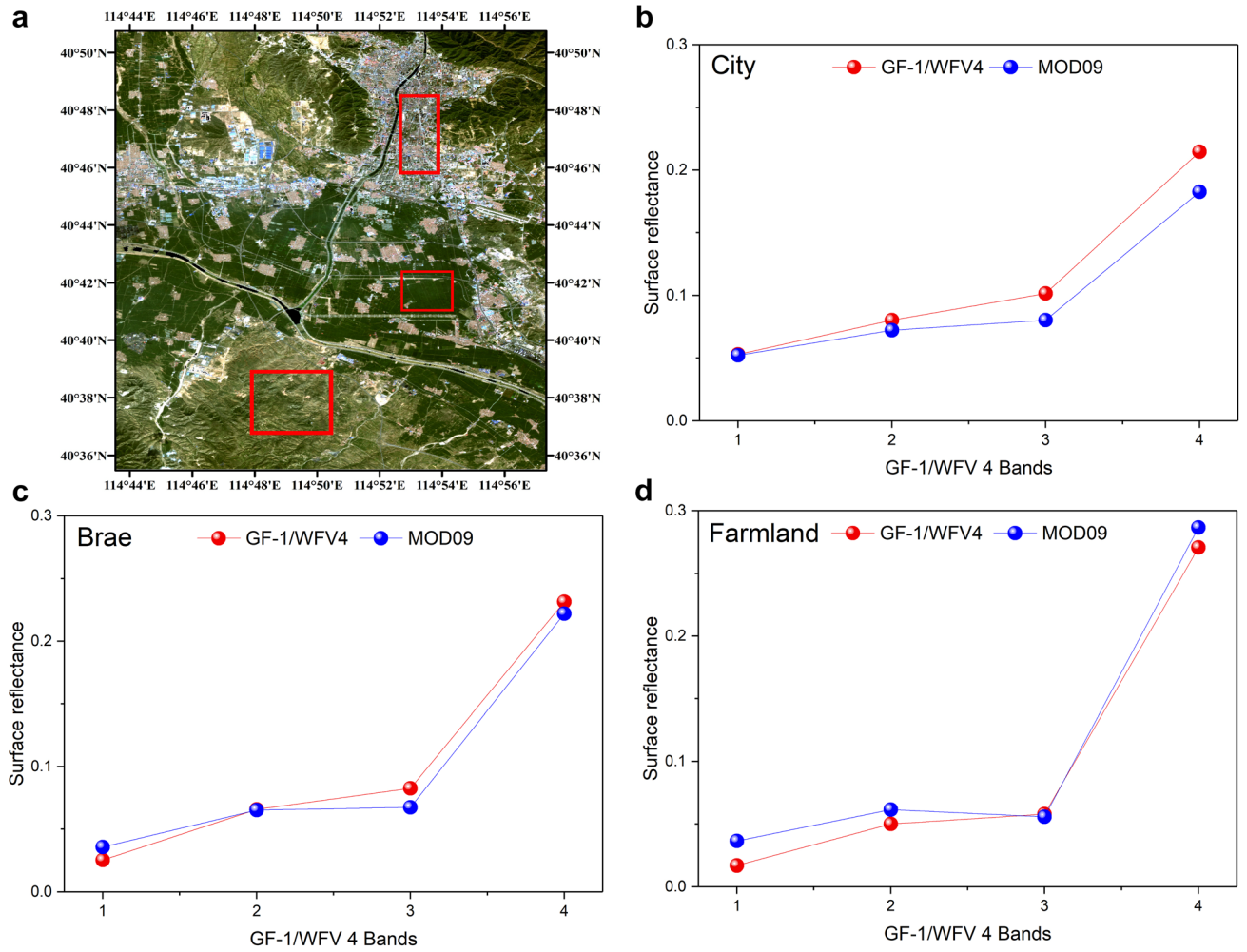

Fig. 6 Validation of the atmospheric correction method via MOD09 surface reflectance. **a** True color image of GF-1/WFV4 after atmospheric correction on September 14, 2015, **b** city, **c** brae and **d** farmland

Uncertainty arises from many different sources during the process of retrieving the surface reflectance. Apart from calibration coefficient, AOD, aerosol type, and related angles, the bidirectional reflectance distribution function (BRDF) is also one of the most important factors in surface reflectance retrieval due to surface anisotropy (Román et al. 2011; Martin et al. 2015). However, due to the existence of only a single-view geometry for the GF-1 satellite WFV4 imagery, we could not analyze the effects of BRDF accuracy on retrieved surface reflectance. In addition, we analyzed only a single sample of each land cover type, which may have also introduced uncertainties in the results.

When compared with the results of Vermote and Vermeulen (1999), differences in the results in the present study may exist because different data sources were employed. One stems from the different spectral response between the WFV4 camera and MODIS imagery (Liang 2000). The WFV4 camera had a broadband spectrum, whereas the MODIS imagery had a narrowband spectrum (Fig. 7a). Figure 7b illustrates that the REs of reflectance between the WFV4 camera and MODIS reached up to − 20.6%. Another is the different surface reflectance observed by the two sensors. In Table 3, the surface reflectance of band 1 is obviously much lower than that of band 4. Based on the analysis in Sect. 3, the uncertainties of the input parameters in the atmospheric correction methods on surface reflectance retrieval for low surface reflectance (e.g., band 1) were almost larger than those for high surface reflectance (e.g., band 4). Therefore, the different surface reflectance between this paper and Vermote and Vermeulen led to different results.

Table 3 The absolute error of AOD accuracy on surface reflectance retrieval

Surface type	Band	Reflectance	Absolute error	
			AOD − (0.05 + 0.15 × AOD)	AOD + (0.05 + 0.15 × AOD)
Shrub	1	0.025	0.012	− 0.014
	2	0.061	0.007	− 0.008
	3	0.07	0.004	− 0.006
	4	0.246	− 0.005	0.004
Corn	1	0.015	0.012	− 0.013
	2	0.05	0.008	− 0.009
	3	0.042	0.006	− 0.007
	4	0.331	− 0.007	0.008
Grass	1	0.04	0.011	− 0.013
	2	0.079	0.005	− 0.007
	3	0.087	0.004	− 0.004
	4	0.351	− 0.008	0.008
Soil	1	0.084	0.007	− 0.01
	2	0.132	0.002	− 0.004
	3	0.191	− 0.001	0.001
	4	0.273	− 0.005	0.006

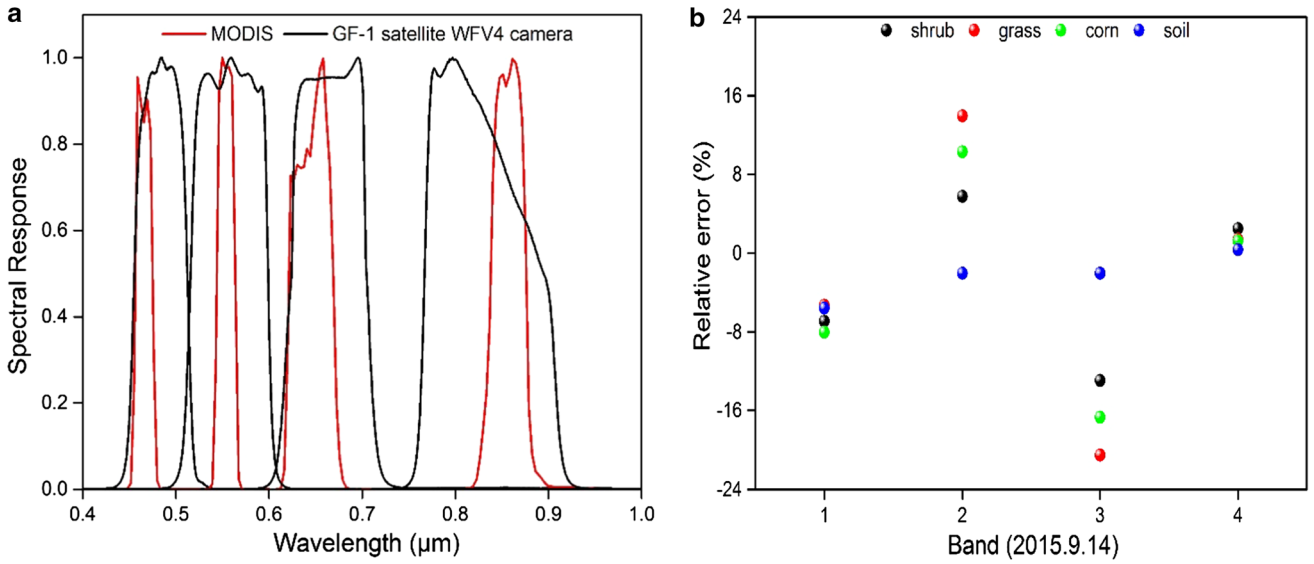

Fig. 7 **a** The spectral response between WFV4 camera and MODIS. **b** The REs of reflectance calculated between the spectra of WFV4 camera and MODIS (September 14, 2015)

Conclusions

To analyze the effects of input parameters in atmospheric correction methods on retrieved surface reflectance acquired from high-spatial-resolution satellite data, we here evaluated the effects of calibration coefficient, AOD, aerosol type, and satellite zenith angle on shrub, corn, grass, and soil reflectance retrieval by using GF-1 satellite WFV4 camera imagery. The results indicated that the effects of satellite zenith angle on retrieved surface reflectance were the smallest of all the input parameters, with REs ranging from − 53.3 to 26.7%. This was followed by the effects of AOD and calibration coefficient, whereas the largest effects stemmed from the aerosol type, with a range of REs from − 14.0 to 286.7% for the four surfaces. Therefore, in order to produce accurate surface reflectance data from WFV4 imagery, we first need to enter in the correct aerosol type, accurately calibrate the coefficient and AOD, and finally the satellite zenith angle as part of the atmospheric correction methodology.

Acknowledgements This work was supported in part by the National Key R&D Program of China (Grant No. 2017YFB0502800), Beijing Natural Science Foundation (Grant Number: 8184087), and the open Fund of State Key Laboratory of Remote Sensing Science (Grant No. OFSLRSS201715). The authors would like to thank CCRSDA for providing GF-1 satellite WFV4 imagery and NASA for providing MOD09 product.

Appendix A: The Characteristics of GF-1 Satellite WFV4 Camera

See Table 4.

Table 4 The characteristics of GF-1 satellite WFV4 camera

Band	Spectrum range (μm)	Spatial resolution (m)	GF-1 temporal resolution (day)	Swath width (km)
1	0.45–0.52	16	4	200
2	0.52–0.59			
3	0.63–0.69			
4	0.77–0.89			

Appendix B: The Geographic Locations of Surfaces

See Table 5.

Table 5 The geographic locations of four surfaces

Surface type	Longitude	Latitude
Shrub	114°50′08.05″–114°50′11.39″	40°42′18.11″–40°42′22.02″
Grass	114°49′24.22″–114°49′25.28″	40°40′56.51″–40°40′57.62″
Corn	114°49′42.03″–114°49′47.25″	40°43′22.17″–40°43′27.78″
Soil	114°50′01.18″–114°50′03.67″	40°42′03.57″–40°42′06.58″

Appendix C: The Effects of Sun Zenith Angle Accuracy on Surface Reflectance Retrieval

See Fig. 8.

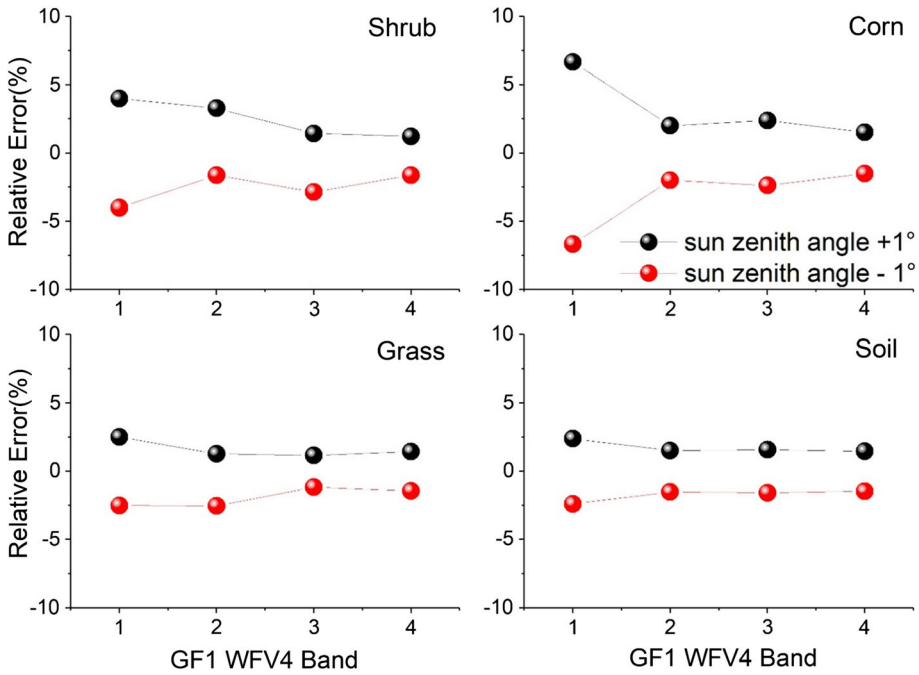

Fig. 8 The effects of sun zenith angle accuracy on the retrieved surface reflectance

Appendix D: The Effects of Azimuth Angle Accuracy on Surface Reflectance Retrieval

See Fig. 9.

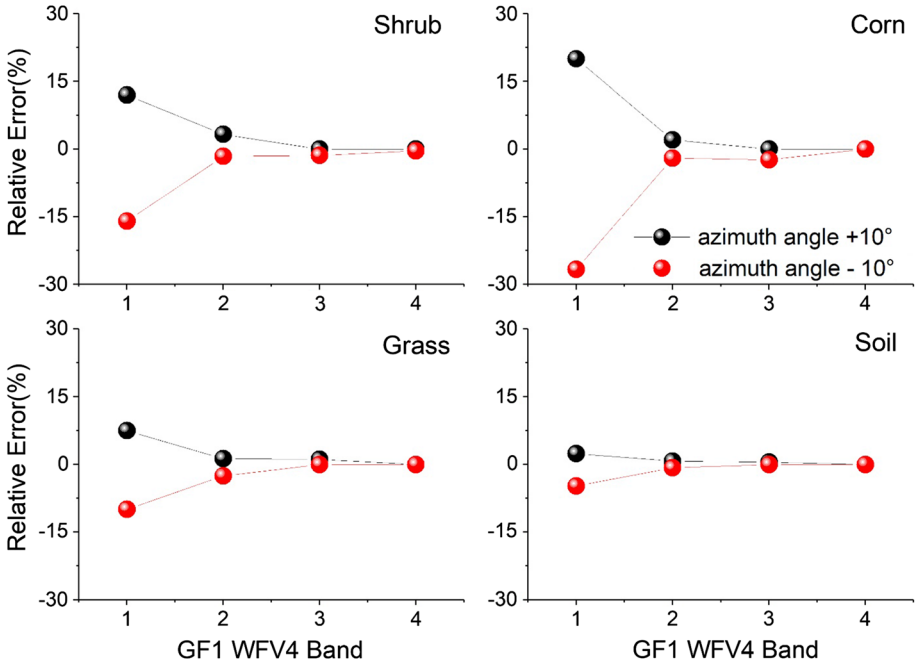

Fig. 9 The effects of azimuth angle accuracy on the retrieved surface reflectance

References

Bai, Z. (2014). The design and characteristics of GF-1 satellite. *Space International, 3,* 12–19.

Baugh, W. M., & Groeneveld, D. P. (2008). Empirical proof of the empirical line. *International Journal of Remote Sensing, 29*(3), 665–672.

Berk, A. (1999). *MODTRAN4 user's manual*. Burlington, MA: Spectral Sciences Inc.

Chavez, P. S. (1996). Image-based atmospheric corrections-revisited and improved. *Photogrammetric Engineering and Remote Sensing, 62*(9), 1025–1036.

Cheng, T., et al. (2009). Effect of surface reflectances on the space-based vector radiative detection. *Acta Physica Sinica*, *58*(10), 7368–7375.

Chrysoulakis, N., et al. (2010). Comparison of atmospheric correction methods using ASTER data for the area of Crete, Greece. *International Journal of Remote Sensing*, *31*(24), 6347–6385.

Clark, B., et al. (2010). A comparison of methods for the retrieval of surface reflectance factor from multitemporal SPOT HRV, HRVIR, and HRG multispectral satellite imagery. *Canadian Journal of Remote Sensing*, *36*(4), 397–411.

Evans, K. F., & Stephens, G. L. (1991). A new polarized atmospheric radiative transfer model. *Journal of Quantitative Spectroscopy & Radiative Transfer, 46,* 413–423.

Gao, H., et al. (2016). Cross-calibration of GF-1 PMS sensor with Landsat 8 OLI and Terra MODIS. *IEEE Transactions on Geoscience and Remote Sensing*, *54*(8), 4847–4854.

Gu, X., & Tong, X. (2015). Overview of China earth observation satellite programs (space agencies). *IEEE Geoscience & Remote Sensing Magazine, 3,* 113–129.

Guo, H., et al. (2014). Evaluation of four dark object atmospheric correction methods based on ZY-3 CCD data. *Spectroscopy and Spectral Analysis*, *34*(8), 2203–2220.

Lee, K. H., & Kim, Y. J. (2010). Satellite remote sensing of Asian aerosols: A case study of clean, polluted, and Asian dust storm days. *Atmospheric Measurement Techniques, 3,* 1771–1784.

Levy, R. C., et al. (2010). Global evaluation of the Collection 5 MODIS dark-target aerosol products over land. *Atmospheric Chemistry and Physics*, *10*, 10399–10420.

Levy, R. C., et al. (2013). The collection 6 MODIS aerosol products over land and ocean. *Atmospheric Chemistry and Physics*, *6*, 2989–3034.

Li, S. S., et al. (2011). Retrieval and validation of the surface reflectance using HJ-1-CCD data. *Spectroscopy and Spectral Analysis*, *31*(2), 516–520.

Li, J., et al. (2016). Radiometric cross calibration of gaofen-1 wfv cameras using landsat-8 oli images: A simple image-based method. *Remote Sensing*, *8*(5), 411.

Liang, S. (2000). Narrowband to broadband conversions of land surface albedo I: Algorithms. *Remote Sensing of Environment, 76,* 213–238.

Mahiny, A. S., & Turner, B. J. (2007). A comparison of four common atmospheric correction methods. *Photogrammetric Engineering and Remote Sensing, 73*(4), 361–368.

Martin, C., et al. (2015). Evaluation of medium spatial resolution BRDF-adjustment techniques using multi-angular SPOT4 (Take5) acquisitions. *Remote Sensing*, *7*, 12057–12075.

Qin, Y., et al. (2015). Characterizing the aerosol and surface reflectance over Australia using AATSR. *IEEE Transactions on Geoscience and Remote Sensing*, *53*(11), 6163–6182.

Román, M., et al. (2011). Variability in surface BRDF at different spatial scales (30 m–500 m) over a mixed agricultural landscape

as retrieved from airborne and satellite spectral measurements. *Remote Sensing of Environment*, *115*, 2184–2203.

Shao, Z., et al. (2018). Performance evaluation of single-label and multi-label remote sensing image retrieval using a dense labeling dataset. *Remote Sensing*, *10*(6), 964.

Tian, Q., et al. (1998). Image-based atmospheric radiation correction and reflectance retrieval methods. *Quarterly Journal of Applied Meteorology*, *9*(4), 456–461.

Tyagi, P., & Bhosle, D. (2011). Atmospheric correction of remotely sensed images in spatial and transform domain. *International Journal of Image Processing, 5*(5), 564–579.

Vaudour, E., et al. (2008). Spatial retrieval of soil reflectance from SPOT multispectral data using the empirical line method. *International Journal of Remote Sensing*, *29*(19), 5571–5584.

Vermote, E. F., et al. (1997). Second simulation of the satellite signal in the solar spectrum: An overview. *IEEE Transactions on Geoscience and Remote Sensing*, *35*(3), 675–686.

Vermote, E. F., & Kotchenova, S. (2008). Atmospheric correction for the monitoring of land surfaces. *Journal Geophysical Research, 113,* D23S90.

Vermote, E. F., & Vermeulen, A. (1999). *Atmospheric correction algorithm: Spectral reflectance (Mod09)*. National Aeronautics and Space Administration. Available online: http://modis.gsfc.nasa.gov/data/atbd/atbd_mod08.pdf.

Wang, Z. T., et al. (2015). Retrieval of AOD from GF-1 16 m camera via DDV algorithm. *Journal of Remote Sensing*, *19*(3), 530–538.

Wang, Z. T., et al. (2016). Quickly atmospheric correction for GF-1 WFV cameras. *Journal of Remote Sensing*, *20*(3), 353–360.

Yang, A., et al. (2015). Cross-calibration of GF-1/WFV over a desert site using Landsat 8/OLI imagery and zy-3/tlc data. *Remote Sensing*, *7*(8), 10763–10787.

Zhang, Z., et al. (2019a). Deep learning based retrieval of forest aboveground biomass from combined LiDAR and landsat 8 Data. *Remote Sensing*, *11*(12), 1459.

Zhang, Z., et al. (2019b). Improved deep hashing with soft pairwise similarity for multi-label image retrieval. *IEEE Transactions on Multimedia*, *2019*(99), 1–14. https://doi.org/10.1109/TMM.2019.2929957.

Zou, Q., et al. (2015). Deep Learning Based Feature Selection for Remote Sensing Scene Classification. *IEEE Geoscience and Remote Sensing Letters*, *12*(11), 2321–2325. https://doi.org/10.1109/LGRS.2015.2475299.

Zou, Q., et al. (2019). DeepCrack: learning hierarchical convolutional features for crack detection. *IEEE Transactions on Image Processing*, *28*(3), 1498–1512.